Available online at www.sciencedirect.com
ScienceDirect
Catalysis Today 123 (2007) 31–36
CATALYSIS TODAY
www.elsevier.com/locate/cattod

The morphology of MoS_2, WS_2, Co–Mo–S, Ni–Mo–S and Ni–W–S nanoclusters in hydrodesulfurization catalysts revealed by HAADF-STEM

M. Brorson *, A. Carlsson, H. Topsøe

Haldor Topsoe, Nymøllevej 55, DK-2800 Kgs., Lyngby, Denmark

Available online 24 April 2007

Abstract

HAADF-STEM studies have provided detailed morphological insight regarding MoS_2, WS_2, Co–Mo–S, Ni–Mo–S and Ni–W–S nanostructures in graphite-supported catalysts. It is found that the technique allows the catalytically active edges to be imaged even for single layer metal sulfide structures. Unpromoted MoS_2 and WS_2 are predominantly present as slightly truncated triangular clusters containing only a single S–M–S layer (M = Mo, W). The addition of promoter atoms results in more heavy truncations consistent with the expected tendency for the Co–Mo–S structures to expose promoted $(\bar{1}\,0\,1\,0)$ S-type edges at the expense of unpromoted $(1\,0\,\bar{1}\,0)$ Mo-type edges. However, the HAADF-STEM (High-Angle Annular Dark-field Scanning Transmission Electron Microscopy) results show for the first time that Co–Mo–S and Ni–W–S may also expose extended high index $(1\,1\,\bar{2}\,0)$ truncations.

Keywords: Nanocluster; Hydrodesulfurization; Co-Mo-S; Ni-Mo-S; Ni-W-S; HAADF-STEM

1. Introduction

There is currently a large interest in the study of MoS_2 and WS_2 nanostructures since they form the basis for the active nanoclusters in industrial hydrotreating and hydrodesulfurization (HDS) catalysts. Such catalysts are used extensively in oil refineries to remove sulfur and other undesirable components from various fractions [1–3]. New legislation demands the production of ultra-low sulfur transport fuels and the drive to improve HDS catalysts has therefore increased considerably in recent years [4–13]. As sulfur conversion goes up, the catalyst is required to handle very refractory compounds like dibenzothiophene (DBT) and, in particular, dialkylated DBTs [2,3,7,8,14]. It has been shown that the conversion of DBT-type molecules may proceed via both a prehydrogenation route (HYD) and a direct desulfurization route (DDS). Under idealized reaction conditions, unsubstituted DBT reacts mainly via the DDS route, whereas the HYD route becomes increasingly important for the more refractory alkyl-substituted DBTs [2,3,7,8]. These results indicate that different types of sites exist at the surfaces of the MoS_2 type nanoclusters and it is clearly highly desirable to gain detailed insight into the nature of the active surfaces. However, despite significant progress in the overall characterization of HDS catalysts [2], it has been difficult to pinpoint the exact location and nature of the active sites in industrial-type catalysts.

In situ studies using techniques, like EXAFS [15–17], show that in typical alumina-supported catalysts Mo is present as small MoS_2 nanocrystals dispersed on the surface of the high surface area support. Bulk MoS_2 has a layer structure in which individual S–Mo–S layers (''slabs'') are stacked on top of each other separated by van der Waal's gaps. It has been shown [18,19] that in many alumina-supported catalysts, the MoS_2 phase is highly dispersed and monolayer or single slab structures may dominate.

While unpromoted MoS_2 (WS_2) catalysts do not possess high catalytic activity, a very significant increase in activity can be achieved by adding Co or Ni [2]. This promotion was shown by in situ Mössbauer emission spectroscopy to be related to the formation of Co–Mo–S type structures [20,21]. These structures and the analogous Ni–Mo–S structures can be considered as MoS_2 structures with the promoter atoms located

* Corresponding author. Tel.: +45 22754653; fax: +45 45272999.
E-mail address: mib@topsoe.dk (M. Brorson).

0920-5861/$ – see front matter © 2007 Elsevier B.V. All rights reserved.
doi:10.1016/j.cattod.2007.01.073

somewhere at the edges of the S–Mo–S layers [22]. The activity was shown to be linked to the presence of the edge promoter atoms. Also for unpromoted catalysts, several structure–activity correlations revealed that the activity is associated with the edges of the MoS_2 structures [2].

In order to gain further insight into the location of the active sites, an understanding of the detailed morphology of the S–Mo–S layers in the MoS_2 nanocrystals must be obtained. However, information regarding this morphology has generally not been available and it has been assumed that the hexagonal morphology observed for macroscopic crystals also applies for the nanocrystals in industrial-type catalysts. If this is the case, there would be equal concentration of $(\bar{1}010)$ (so-called S edges) and $(10\bar{1}0)$ (so-called Mo edges).

Many researchers have used high-resolution transmission electron microscopy (HRTEM) in order to obtain morphological insight into HDS catalysts [23–38]. However, such experiments do not provide detailed answers and very small clusters may not be imaged at all [25,31,33]. Also in HRTEM experiments, individual S–Mo–S layers are typically only imaged when they are oriented essentially edge-on relative to the electron beam, i.e. the layers are viewed as lines. Due to a very low contrast, top view imaging of single layers has only been possible for high surface area catalysts in special instances [39]. Thus, HRTEM studies have not been able to provide insight into the morphology of the layers, and information regarding the abundance of different types of edges has thus not been available. In the absence of this information, both unpromoted and promoted MoS_2 (WS_2) nanocrystals have, as mentioned above, typically been assumed to exhibit the bulk-like hexagonal morphology.

Recent scanning tunnelling microscopy (STM) studies of Au(1 1 1)-supported MoS_2 nanocrystals showed that they may not display the hexagonal morphology [40]. Also, the presence of Co promoter atoms was found to change the MoS_2 morphology [41], and density functional theory (DFT) calculations [42] suggest that this is due to a preference for Co to be located at the $(\bar{1}010)$ edges (so-called S edges). The STM model catalyst studies [43] also show that the composition of the adjoining atmosphere may influence the morphology. This is in accordance with DFT calculations, which showed that the morphology and the edge structures may depend on the reaction conditions [42,44,45].

The model catalyst studies and the theoretical studies have provided interesting new insight and they further emphasize the need to obtain morphological insight for more realistic high surface area catalysts. Recently, we showed that the morphology of single layer S–W–S layers could be observed in a high surface area graphite-supported catalyst using high-angle annular dark-field scanning transmission electron microscopy (HAADF-STEM) [39]. This technique, which was first applied in dedicated STEM instruments [46–50], uses electron scattering at high angles to create a *Z*-contrast image. In order to obtain full advantage of the technique, we studied a system consisting of the heavy element sulfide, WS_2, on the light element support, graphite. Most industrial HDS catalysts are based on MoS_2 rather than WS_2. The present study show that important morphological information can also be obtained for MoS_2 based catalysts even when MoS_2 is present as single layer structures. Some preliminary results were presented in Ref. [51]. The present study will also discuss HAADF-STEM results for Ni and Co promoted MoS_2 systems.

2. Experimental

Graphitic carbon (Timcal Timrex HSAG100 CAT, Special Graphite, M-292) with a BET surface area of 118 m^2/g was used as support. After tabletizing, the carbon powder was granulated and then impregnated by the incipient wetness method with an aqueous solution containing $(NH_4)_2[MS_4]$ (M = Mo or W) and, in case of the promoted catalysts, also $Me(acetate)_2$ (Me = Co, Ni). When promoter atoms were present in the liquids, the relatively low target loads combined with a quick working procedure prevented precipitation before impregnation. Samples were dried in air at 110 °C. The atomic ratio M:Me was for the promoted catalysts 3, and the Mo(W) loading was around 0.3 wt% (0.6 wt%), i.e. identical *molar* loadings of Mo and W. The samples were treated with 10% H_2S in H_2 for 6 h at 1073 K, cooled to room temperature in N_2, and then passivated by means of 1% O_2 in N_2 before they were quickly transferred from the cold tube furnace to a container where they were stored under N_2 until TEM analysis. For TEM analysis the samples were crushed in a mortar and deposited dry on standard Cu TEM-grids covered with lacey carbon. HAADF-STEM measurements were performed on a Philips CM200 FEG UltraTwin electron microscope, with a primary electron energy of 200 keV, $C_s = 0.5$ mm and a point-to-point resolution of 1.9 Å in TEM mode. The resolution in STEM mode depends on the instrument settings used, but the images presented here have a resolution of ca 0.4 nm, as determined from the observation of lattice fringes. The alignment for STEM was carried out using ronchigrams [52]. The contrast in HAADF images is approximately proportional to $Z^{1.7}$ [50], and this is thus an excellent technique for observing heavy nanoparticles (e.g. MoS_2 or WS_2) on a light support (e.g. C).

3. Results and discussion

The preparation procedure employed in the present work is based on impregnation with aqueous solutions of ammonium tetrathiometallate compounds, $(NH_4)_2[MS_4]$ (M = Mo, W). This is different from the method employed previously [39], where the oxidic precursor compound ammonium metatungstate, $(NH_4)_6[H_2W_{12}O_{40}]$, was used for impregnation. However, we find that the use of sulfidic precursors gives rise to more of the well-ordered regular MS_2 structures. The impregnated and dried samples were treated with 10% H_2S in H_2 at 1073 K in order to promote full sulfidation of the metals as well as equilibration of the nanocluster structures. The more prevalent regular structures obtained by this new impregnation method allow a more detailed investigation of the effects of promoter atoms on the morphology.

Fig. 1 shows an overall view of an ensemble of regularly shaped MoS_2 clusters located on a graphite sheet oriented

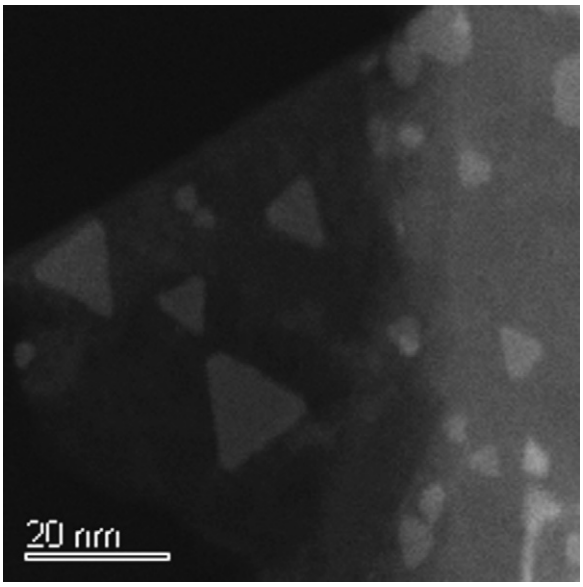

Fig. 1. HAADF-STEM image of MoS_2 clusters supported on a thin graphite sheet oriented more or less perpendicular to the line of observation. Many of the clusters display a highly regular, slightly truncated triangular morphology.

nearly perpendicular to the line of sight. One goal of the present study was to establish whether HAADF-STEM could be used to image MoS_2 which is somewhat lighter than WS_2 studied previously [39]. Fig. 1 shows that this is indeed the case—even when MoS_2 occurs as single-layer structures (see below). The high degree of regularity displayed in, for example, Fig. 1 also means that general statements concerning cluster morphology can be made on a solid basis.

It is surprising that in spite of the preparative procedure employed and the high temperature used in sulfiding/equilibration, many of the clusters observed are still irregular and/or contain defects. In many cases, the shape of the clusters is clearly directed by irregularities, e.g. steps, in the graphite support. This situation is quite different from what was observed by STM for the MoS_2 on Au(1 1 1) model system [40]. Here a very high degree of morphology regularity was seen. Clearly, the graphitic carbon used here does not provide surfaces nearly as perfect as those on gold single crystals. In this way the results for the carbon-supported catalysts probably resemble more closely those expected for industrial alumina-supported catalysts where the lower sulfidation/equilibration temperatures typically employed may be expected to further increase the degree of irregularity.

The individual MoS_2 (WS_2) clusters are imaged as bright patches (ca. 1–100 nm in diameter) on the graphite support, which is mostly present as thin sheets with a thickness of 5–10 nm. A key question in hydrotreating catalysis is whether MoS_2 is present as single or multiple S–Mo–S layer structures [2]. The HAADF-STEM technique readily allows determination of the number of S–Mo–S (S–W–S) layers in the MoS_2 (WS_2) clusters from the intensity levels, which are observed to increase in even steps [39]. Paired with the observation that the thinnest clusters imaged edge–on are predominately single layer structures this allows for unambiguous determination of the number of layers in the individual particles [39]. It was found that the vast majority of nanoclusters observed in the current study were of the single-layer type. When areas of higher image intensity are sometimes observed they are either due to particles with multilayer structures or to coincidental overlap along the line of vision of single-layer structures located on opposite sides of a graphite sheet. In Ref. [39] we recorded an edge-on view, which provides direct evidence for the latter situation. The image contrast for MoS_2 clusters is lower than for WS_2, as can be expected from the $Z^{1.7}$ dependence, but even single layer MoS_2 particles are imaged with good contrast and acceptable noise levels as shown in Fig. 1.

Fig. 2 shows close-ups of MoS_2 clusters (a) and WS_2 clusters (b) on catalysts prepared analogously. Again the images have

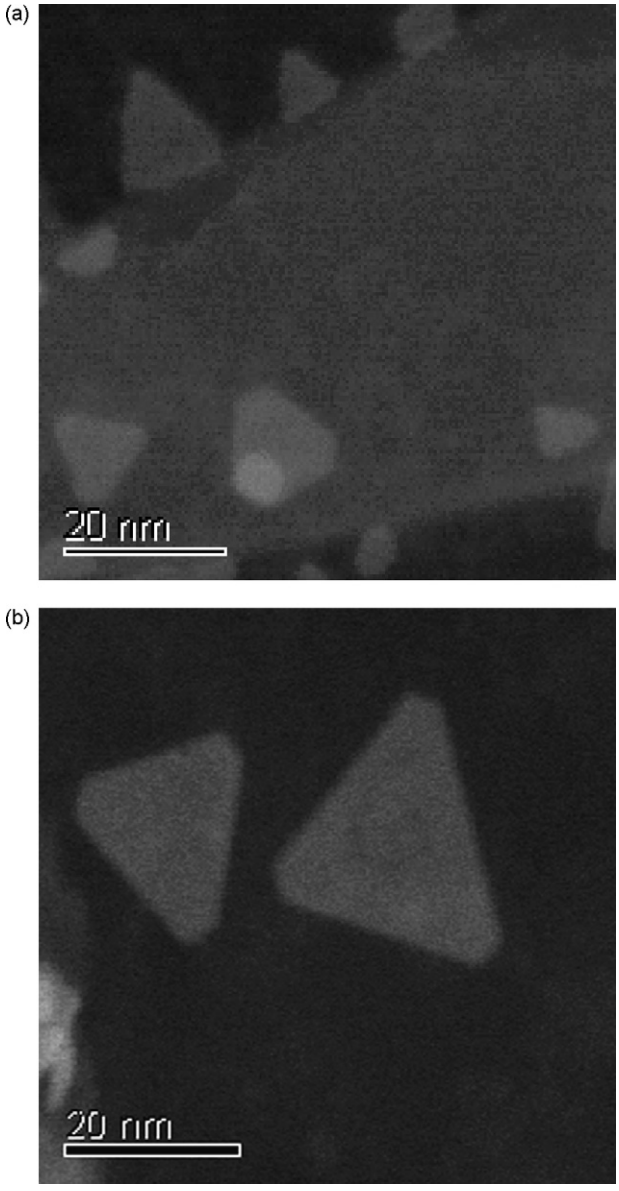

Fig. 2. Close-up HAADF-STEM images of MoS_2/graphite (a) and WS_2/graphite (b) catalysts made in analogous ways and with identical molar metal loadings. Although the WS_2 as expected is imaged with higher contrast than MoS_2, the morphology of MoS_2 clusters is clearly observed. All clusters in these images are single-layer structures.

been selected to show nanoclusters on graphite sheets that happen to be oriented more or less perpendicular to the line of vision. In general, the MoS_2 clusters were observed to be smaller than WS_2 clusters prepared under identical conditions. This is somewhat surprising and certainly not in accordance with what would be expected based on traditional mass-dependent mobility and sintering rates. The most common regular shape for these unpromoted MoS_2(WS_2) clusters is that of a truncated triangle. The $\sim 120^\circ$ angles displayed at the vertices of the nanostructures are consistent with both the $(1\,0\,\bar{1}\,0)$ (so-called Mo(W) edges) and $(\bar{1}\,0\,1\,0)$ (so-called S edges) being exposed. Recent STM and DFT studies have provided insight into the detailed structure of these edges [40,42,44,45].

In the first STM study [40] of unpromoted MoS_2 clusters on gold surfaces, it was observed that the prevalent morphology was that of triangles with only the $(1\,0\,\bar{1}\,0)$ edges exposed. However, later studies [43] showed that the MoS_2 morphology depended on the composition of the atmosphere in which the particles were synthesized. It was thus found that regular triangles dominate when the nanocluster synthesis was conducted in an atmosphere of essentially pure H_2S (H_2S:H_2 = 500). However, the presence of substantial amounts of H_2 in the synthesis mixture (H_2S:H_2 = 0.07) led to a preferred MoS_2 morphology closer to hexagonal, i.e. severely truncated triangles. The present HAADF-STEM results clearly show the presence of truncated triangular nanocrystallites. The atmosphere under which the STM samples were produced (H_2S:H_2 = 0.07) is very close to that used for our current experiments (H_2S:H_2 = 0.11). It is interesting that some of the morphology changes observed in the STM model system [43] and also calculated theoretically [44,45] are also found in the HAADF-STEM experiments for the more realistic catalysts. The fact that the morphologies observed in the two kinds of experiments are not identical is not surprising. Considering the vastly different synthetic conditions used for synthesis (STM uses e-beam deposition of Mo atoms in a 2×10^{-6} bar atmosphere), it is actually remarkable that the observed morphologies are so relatively similar. One reason for this may be that both the perfect graphite and Au(1 1 1) surfaces interact weakly with the MoS_2 nanoclusters.

Promoted catalysts are more interesting from an industrial perspective and Figs. 3 and 4 show that HAADF-STEM can also provide important morphological insight into the Co–Mo–S type structures. The catalyst samples imaged were sulfided in exactly the same way as the unpromoted samples discussed above; promoter atoms were present in the impregnation liquids in a concentration one-third of Mo (W). From the images it is immediately clear that the addition of promoter atoms modifies the cluster morphology. When Ni or Co is present in the MoS_2 samples, more heavily truncated triangular morphologies are observed (Fig. 3). Moreover, the truncations of the triangles observed both in the case of Ni and Co are clearly different from what is seen in the unpromoted catalysts (Figs. 1 and 2).

The presence of the promoter atoms is seen to result in several changes in the morphology. The HAADF-STEM results show that the degree of truncation increases such that the

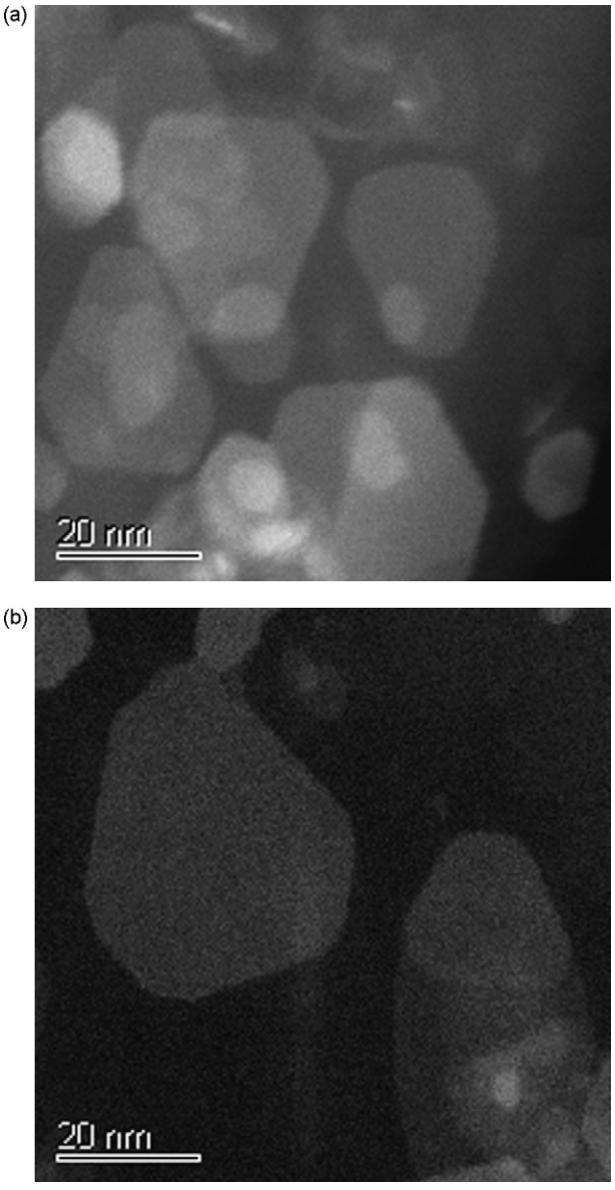

Fig. 3. Promotion of MoS_2 nanoclusters with Ni (a) or Co (b) changes to morphology towards that of regular hexagons, i.e. heavily truncated triangles. The image (a) displays accidental overlap of clusters located along the same line of observation, possibly clusters located at opposite sides of the same graphite sheet. The corners of both Ni–Mo–S (a) and Co–Mo–S (b) structures appear rounded due to additional truncations that expose high-index edges.

morphology changes towards being more hexagonal. This was also observed for Co-promoted MoS_2 nanoclusters on Au(1 1 1) by STM [41] and it was explained by DFT calculations [42] which showed the Co atoms in the Co–Mo–S structures to be located at the $(\bar{1}\,0\,1\,0)$ S edges. The presence of Co will cause MoS_2 nanoparticles to expose more promoted $(\bar{1}\,0\,1\,0)$ S-type edges at the expense of unpromoted $(1\,0\,\bar{1}\,0)$ Mo-type edges. The present results indicate that this is also the situation for Ni–Mo–S (Fig. 3a) and Ni–W–S (Fig. 4).

It is interesting that the HAADF-STEM results show that the promoter atoms may have other effects than influencing the degree of truncation and the concentration of promoted $(\bar{1}\,0\,1\,0)$ S-type edges. Instead of the exclusive presence of 120° angles

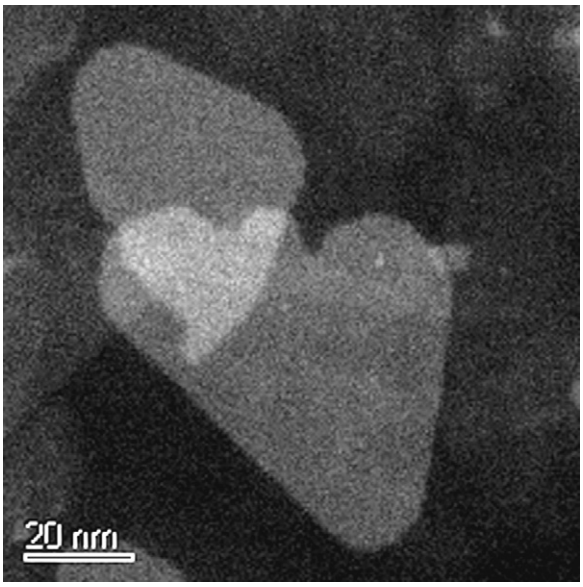

Fig. 4. Promotion of WS_2 nanoclusters with Ni gives, as in Co–Mo–S and Ni–Mo–S structures, rise to additional truncations that expose high-index edges. Close to the bottom of the image these additional truncations are seen as straight lines that form angles with the main triangular edges consistent with an assignment [53] as $(1\,1\,\bar{2}\,0)$ edges.

between the edges (indicating the presence of only $(1\,0\,\bar{1}\,0)$ and $(\bar{1}\,0\,1\,0)$ edges) we now also observe particles with more rounded truncations. In several cases it is clear that the additional new higher index edges are present. Some of them have angles of about 150° to the dominant edges and it is likely that the promoted structures also expose $(1\,1\,\bar{2}\,0)$ edges. Indications for this was also found in atomically resolved STM images of Ni–Mo–S structures [53] but in those studies the $(1\,1\,\bar{2}\,0)$-like facts only extended for a few atoms and a clear detection was difficult. The present results show that extended $(1\,1\,\bar{2}\,0)$ edges may indeed be stable features of the promoted structures. The STM studies only observed the high index truncations for small clusters in Ni-promoted MoS_2 model catalysts [53]. It is interesting that we observe presently high index truncations also for large clusters. Furthermore, Co and Ni have a similar effect on the shape of the MoS_2 clusters. The presence of high index truncations is furthermore also seen for Ni-promoted WS_2 clusters (Fig. 4). Thus, the high index truncations may be a common feature for many Co–Mo–S type structures.

4. Conclusion

The HAADF-STEM technique has been found to allow an unambiguous determination of the morphology of the S–Mo–S (S–W–S) layers in MoS_2/C, WS_2/C, Co–Mo–S/C, Ni–Mo–S/C and Ni–W–S/C catalysts. This information allows detailed insight into the type and abundance of different edges present in supported catalysts. Previously, such experimental information was only available from STM studies of model catalyst systems. The current approach also allows one to study the effects of the nature of the active metal precursors and the choice of preparation and sulfiding conditions. This is important since non-equilibrium structures are obtained. Furthermore, by means of the HAADF-STEM technique a study of catalysts that have been retrieved from the environment of high-pressure hydrotreating reactors should also be possible. The preparation procedure used in the current study, where all elements, including sulfur, are introduced in the impregnation step, gives more regular clusters than the standard procedure, where sulfur is introduced only during sulfidation. The most common regular structure observed for $MoS_2(WS_2)$ was truncated triangular, exposing $(1\,0\,\bar{1}\,0)$ Mo(W) edges and $(\bar{1}\,0\,1\,0)$ S edges. The addition of Co or Ni promoter atoms modifies the shape of the clusters, to one closer to hexagonal. This is consistent with the tendency for the Co–Mo–S type clusters to expose more promoted $(\bar{1}\,0\,1\,0)$ S-type edges and it is in accord with STM and DFT studies [41,42]. However, it is of particular interest that HAADF-STEM results show that the Co–Mo–S, Ni–Mo–S and Ni–W–S clusters may expose additional high index facets (like $(1\,1\,\bar{2}\,0)$). The STM studies have only provided evidence for such truncations in very small Ni–Mo–S clusters and they are completely new in the case of the Co–Mo–S and Ni–W–S structure. Clearly such insight must be taken into account when catalytic hydrotreating reactions are to be understood at the molecular level. Finally, the HAADF-STEM technique provides the opportunity for future studies of the influence of different sulfiding agents on the morphology of the catalytic nanostructures formed and of how these morphologies may be influenced by the carbon compounds present in the feed during catalyst operation in a hydrotreating reactor.

References

[1] R. Prins, V.H.J. de Beer, G.A. Somorjai, Catal. Rev. Sci. Eng. 31 (1989) 1.
[2] H. Topsøe, B.S. Clausen, F.E. Massoth, in: J.R. Anderson, M. Boudart (Eds.), Hydrotreating Catalysis, Science and Technology, vol. 11, Springer, Berlin, 1996.
[3] T. Kabe, A. Ishihara, W. Qian, Hydrodesulfurization and Hydrodegeneration, Chemistry and Engineering, Wiley–VCH, Kodanska, 1999.
[4] A. Amorelli, Y.D. Amos, C.P. Halsig, J.J. Kosman, R.R.J. Jonke, M. DeWind, J. Vrieling, Hydrocarb. Process. 71 (1992) 93.
[5] I. Mochida, K. Sakanishi, X. Ma, S. Nagao, T. Isoda, Catal. Today 29 (1996) 185.
[6] M.V. Landau, Catal. Today 36 (1997) 393.
[7] B.C. Gates, H. Topsøe, Polyhedron 16 (1997) 3213.
[8] D.D. Whitehurst, T. Isoda, I. Mochida, Edv. Catal. 42 (1998) 345.
[9] K.G. Knudsen, B.H. Cooper, H. Topsøe, Appl. Catal. A 189 (1999) 205.
[10] H. Schulz, W. Bohringer, P. Waller, F. Ousmanov, Catal. Today 49 (1999) 87.
[11] I.V. Babich, J.A. Moulijn, Fuel 82 (2003) 607.
[12] C. Song, Catal. Today 86 (2003) 211.
[13] T.C. Ho, Catal. Today 98 (2004) 3.
[14] M. Breysse, G. Djega-Mariadassou, S. Pessayre, C. Geantet, M. Vrinat, G. Perot, M. Lemaire, Catal. Today 84 (2003) 129.
[15] B.S. Clausen, H. Topsøe, R. Candia, J. Villadsen, B. Lengeler, J. Als-Nielsen, F. Christensen, J. Phys. Chem. 85 (1982) 3868.
[16] T.G. Parham, R.P. Merrill, J. Catal. 85 (1984) 295.
[17] S.M.A.M. Bouwens, R. Prins, V.H.J. de Beer, D.C. Koningsberger, J. Phys. Chem. 94 (1990) 3711.
[18] N.-Y. Topsøe, J. Catal. 64 (1980) 235.
[19] J. Grimblot, P. Dufresne, L. Gengembre, J.-P. Bonelle, Soc. Chim. Belg. 90 (1981) 1311.

[20] H. Topsøe, B.S. Clausen, R. Candia, C. Wivel, S. Mørup, J. Catal. 68 (1981) 433.
[21] C. Wivel, R. Candia, B.S. Clausen, S. Mørup, H. Topsøe, J. Catal. 68 (1981) 453.
[22] N.Y. Topsøe, H. Topsøe, J. Catal. 84 (1983) 386.
[23] J.V. Sanders, Phys. Scr. 14 (1978–1979) 141.
[24] J.M. Thomas, G.R. Millward, L.A. Bursell, Philos. Trans. R. Soc. A 300 (1981) 43.
[25] R. Candia, O. Sørensen, J. Villadsen, N.-Y. Topsøe, B.S. Clausen, H. Topsøe, Bull. Soc. Chem. Belg. 93 (1984) 763.
[26] F. Delannay, Appl. Catal. 16 (1985) 135.
[27] T.F. Hayden, J.A. Dumesic, J. Catal. 103 (1987) 366.
[28] J. Ramirez, S. Fuentes, G. Diaz, M. Vrinat, M. Breysse, M. Lacroix, Appl. Catal. 52 (1989) 6501.
[29] E. Payen, S. Kasztelaan, S. Houssenbay, R. Szymanski, J. Grimblot, J. Phys. Chem. 93 (1989) 6501.
[30] S. Srinivasan, A.K. Datye, C.H.F. Peden, J. Catal. 137 (1992) 513.
[31] S. Eijsbouts, J.J.L. Heinerman, H.J.W. Elzerman, Appl. Catal. A 105 (1993) 53.
[32] P.L. Hansen, H. Topsøe, J.O. Malm, Proceeding of the 13th International Conference on Electron Microscopy, vol. 2B, Paris, (1994), p. 1077.
[33] R.M. Stockmann, H.W. Zandbergen, A.D. van Langeveld, J.A. Moulijn, J. Mol. Catal. A 102 (1995) 147.
[34] S. Eijsbouts, Appl. Catal. A 158 (1997) 53.
[35] P. Da Silva, N. Marchal. V. Harlé, T. Cseri, S. Kasztelaan, ACS Pet., p. 20 (Preprint, 1998).
[36] Y. Sakushita, T. Yoneda, J. Catal. 185 (1999) 487.
[37] H.R. Reinhoudt, A.D. van langeveld, P.J. Kooyman, R.M. Stockmann, R. Prins, H.W. Zandbergen, J.A. Moulijn, J. Catal. 179 (1998) 443.
[38] P.J. Kooyman, E.J.M. Hensen, A.M. de Jong, J.W. Niemantsverdriet, J.A.R. van Veen, Catal. Lett. 74 (2001) 49.
[39] A. Carlsson, M. Brorson, H. Topsøe, J. Catal. 227 (2004) 530.
[40] S. Helveg, J.V. Lauritsen, E. Lægsgaard, I. Stensgaard, J.K. Nørskov, B.S. Clausen, H. Topsøe, F. Besenbacher, Phys. Rev. Lett. 84 (2000) 951.
[41] J.V. Lauritsen, S. Helveg, E. Lægsgaard, I. Stensgaard, B.S. Clausen, H. Topsøe, F. Besenbacher, J. Catal. 197 (2001) 1.
[42] L.S. Byskov, J.K. Nørskov, B.S. Clausen, H. Topsøe, J. Catal. 187 (1999) 109.
[43] J.V. Lauritsen, M.V. Bollinger, E. Lægsgaard, K.W. Jacobsen, J.K. Nørskov, B.S. Clausen, H. Topsøe, F. Besenbacher, J. Catal. 2221 (2004) 510.
[44] H. Schweiger, P. Raybaud, H. Toulhaut, J. Catal. 212 (2002) 33.
[45] M.V. Bollinger, K.W. Jacobsen, J.K. Nørskov, Phys. Rev. B 67 (2003) 085410.
[46] A.V. Crewe, J.P. Wall, J.P. Langmore, Science 168 (1970) 1138.
[47] M.M. Treacy, A. Howie, S.J. Pennycook, Inst. Phys. Conf. Ser. 52 (1980) 261.
[48] J.M. Thomas, O. Terasaki, Top. Catal. 21 (2002) 155.
[49] A.K. Datye, J. Catal. 216 (2003) 144.
[50] S. Hillyard, J. Silcox, Ultramicroscopy 58 (1995) 6.
[51] A. Carlsson, M. Brorson, H. Topsøe, J. Microsc. 223 (2006) 179.
[52] E.M. James, N.D. Browning, Ultramicroscopy 78 (1999) 125–139.
[53] J.V. Lauritsen, J. Kibsgaard, G.H. Olesen, P.G. Moses, B. Hinnemann, J.K. Nørskov, B.S. Clausen, H. Topsøe, E. Lægsgaard, F. Besenbacher, submitted for publication.